

Hardware Impaired Ambient Backscatter NOMA Systems: Reliability and Security

Xingwang Li, *Senior Member, IEEE*, Mengle Zhao, *Student Member, IEEE*, Ming Zeng, *Member, IEEE*, Shahid Mumtaz *Senior Member, IEEE*, Varun G Menon *Senior Member, IEEE*, Zhiguo Ding, *Fellow, IEEE*, Octavia A. Dobre *Fellow, IEEE*

Abstract—Non-orthogonal multiple access (NOMA) and ambient backscatter communication have been envisioned as two promising technologies for the Internet-of-things due to their high spectral efficiency and energy efficiency. Motivated by this fact, we consider an ambient backscatter NOMA system in the presence of a malicious eavesdropper. Under some realistic assumptions of residual hardware impairments (RHIs), channel estimation errors (CEEs) and imperfect successive interference cancellation (ipSIC), we investigate the physical layer security (PLS) of the ambient backscatter NOMA systems focusing on reliability and security. In order to further improve the security of the considered system, an artificial noise scheme is proposed where the radio frequency (RF) source acts as a jammer that transmits interference signal to the legitimate receivers and eavesdropper. On this basis, the analytical expressions for the outage probability (OP) and the intercept probability (IP) are derived. To gain more insights, the asymptotic analysis and diversity orders for the OP in the high signal-to-noise ratio (SNR) regime are carried out, and the asymptotic behaviors of the IP in the high main-to-eavesdropper ratio (MER) region are explored as well. Numerical results show that: 1) RHIs, CEEs and ipSIC have negative effects on the OP but positive effects on the IP; 2) Compared with CEEs, RHIs have a more serious impact on the reliability and security of the considered system; 3) There exists a trade-off between reliability and security, and this trade-off can be optimized by reducing the power coefficient of the artificial noise or increasing the interfering factor of readers; 4) There are error floors for the OP due to the CEEs and the reflection coefficient; 5) As MER grows large, the security for R_n and R_f is improved, while the security for T is reduced.

Index Terms—Internet-of-things, ambient backscatter, NOMA, residual hardware impairments, physical layer security, channel estimation errors, imperfect successive interference cancellation, artificial noise.

I. INTRODUCTION

A large number of intelligent devices will be supported for the wireless networks with Internet-of-things (IoT) and

X. Li and M. Zhao are with the School of Physics and Electronic Information Engineering, Henan Polytechnic University, Jiaozuo, China (email:lixingwangbupt@gmail.com, zhaomenglehpu@163.com) (First corresponding author: Xingwang Li).

M. Zeng is with Memorial University, St.John's, NL A1B 3X9, Canada (email: mzeng@mun.ca).

S. Mumtaz is with Institute of Telecommunications, Aveiro, Portugal, (email: smumtaz@av.it.pt).

V. G. Menon is with Department of Computer Science and Engineering, SCMS School of Engineering and Technology, India. (email: varunmenon@ieee.org).

Z. Ding is with the School of Electrical and Electronic Engineering, The University of Manchester, Manchester, UK (email: zhiguo.ding@manchester.ac.uk).

O. A. Dobre is with Memorial University, St. John's, NL A1B 3X9, Canada (e-mail: odobre@mun.ca).

massive machine-type communication [1, 2]. To this end, non-orthogonal multiple access (NOMA) has been identified as a promising solution to serve massive connections due to high spectral efficiency and low latency [3].¹ The distinguishing feature of NOMA is that a plurality of users are allowed to occupy the same time/frequency/code resources by power multiplexing through superposition coding [4]. At the receiver, the signals can be extracted with the aid of successive interference cancellation (SIC) [5]. From the perspective of coverage, NOMA can enhance the performance of the cell edge users by allocating more power to them [6].

On a parallel avenue, backscatter communication has emerged as a promising paradigm for green sustainable IoT applications due to its ultralow-power and low cost [7]. A well-known backscatter communication application for the IoT is radio frequency identification (RFID) that consists of one reader and one tag. More exactly, the tag modulates and reflects the incident signal from the energy source through a mismatched antenna impedance to passively transmit information, and the reader performs demodulation after receiving the reflected signal [8]. However, the traditional backscatter communication technology is limited by the power consumption resulting from the active transmission [9]. To tackle this limitation, the work in [10] proposed ambient backscatter prototypes. This technology utilizes environmental wireless signals (e.g., digital TV broadcasting or cellular signals) to collect energy and transmit information through battery-free tags.

Ambient backscatter technology has drawn great attention from both academia and industry [11–15]. A framework for evaluating the ultimate achievable rates of point-to-point networks with ambient backscatter devices was proposed in [11], where the impact of the backscatter transmission on the performance of the legacy systems was considered. In [12], the authors analyzed the outage performance of the ambient backscatter communication systems with a pair of passive tag-reader by deriving the exact and asymptotic expressions for the outage probability (OP). Guo *et al.* in [13] exploited the NOMA technology to support massive tag connections. According to the unique characteristics of the cooperative ambient backscatter system, the authors of [14] proposed three symbiotic transmission schemes, where the relationships between the primary and backscatter transmissions were

¹Generally, NOMA can be divided into code-domain NOMA and power-domain NOMA. In this paper, we use NOMA to refer to the power-domain NOMA.

commensal, parasitic, and competitive. The authors in [15] investigated the effects of co-channel interference and the energy harvesting (EH) on the achievable OP of the ambient backscatter communication systems with multiple backscatter links.

Another well-known fact is that the transmission of wireless signals is vulnerable to fronted threats due to the broadcast nature of wireless medium. The traditional key encryption technologies has high computation complexity, and thus, are not suitable for small-volume backscatter devices with limited storage and computing power [16]. As a result, they may not be applied for solving the security communication problem of the ambient backscatter NOMA systems [17].

As an alternative, physical layer security (PLS) was proposed as a promising mechanism to ensure the security of wireless communication systems from an information theoretic perspective [18, 19]. By exploiting the inherent random characteristics of wireless channels, PLS can achieve secure communication for wireless networks without being eavesdropped by illegal eavesdroppers, which has sparked a great deal of research interests, e.g., see [20–24] and the references therein. In [20], the secrecy outage performance of a multiple-relay NOMA network was investigated, where three relay selection schemes were proposed. With the emphasis on the cognitive radio networks (CRNs), the authors of [21] evaluated the reliability-security tradeoff by deriving the connection outage probability and the secrecy outage probability for the cooperative NOMA aided CRN systems. Additionally, the secrecy rate was studied under the traditional backscatter communications systems in [22], where the reader and eavesdropper were equipped with multiple antennas. To enhance the security of the ambient backscatter communication systems, an optimal tag selection scheme for the multi-tag ambient backscatter systems was designed in [23]. By the virtue of artificial noise, an enhanced PLS scheme for multi-tag ambient backscatter system was designed, and the bit error rate and secrecy rate were investigated in [24]. Moreover, the authors of [25] proposed to combined multiple-input multiple-output technology with artificial noise technology to enhance the secrecy performance of NOMA systems.

Unfortunately, the common feature of the aforementioned contributions is that perfect radio frequency (RF) components are assumed, which may not be realistic in practical communication systems. In practice, all RF front-ends are vulnerable to several types of hardware impairments due to the configuration of low cost, low-power dissipation, and small size components, such as amplifier non-linearities, in-phase/quadrature imbalance, phase noise, and quantization error [26–28]. These impairments can be generally eliminated by using some compensation and calibration algorithms. However, owing to some factors such as estimation errors, inaccurate calibration, and time-varying hardware characteristics, there are still some residual hardware impairments (RHIs), which can be modeled as an additive distortion noise to the transmitted/received signals [26]. To this end, a great deal of works have studied the impact of RHIs on system performance [28, 29]. In [28], the authors investigated the effects of RHIs on the achievable sum rate of the unmanned aerial vehicle-

aided NOMA relaying networks. Considering two types of relay selection schemes, the impacts of RHIs on the multiple-relay amplify-and-forward network was studied by deriving the tight closed-form expressions for the OP [29].

Moreover, another limitation of the above research works is that imperfect channel state information (CSI) is assumed available at receivers, which is not practical. In fact, it is a great challenge to obtain perfect channel knowledge due to channel estimation errors (CEEs) and feedback delay [30]. The related research works about imperfect CSI have been reported in [31–33]. The outage performance of the down-link cooperative NOMA systems based on wireless backhaul unreliability and imperfect CSI was studied by deriving the exact and asymptotic OP expressions at the receivers [31]. A proportional fair scheduling algorithm was proposed to achieved high throughput and fairness, which was extended to the multi-user NOMA scenarios with imperfect CSI in [32]. The authors of [33] considered a more practical scenarios, where the outage performance of the amplify-and-forward relay systems was analyzed in the presence of RHIs and CEEs. Therefore, it is of high practical relevance to look into the realistic scenario with imperfect CSI and RHIs.

A. Motivation and Contribution

The previous research works have laid a solid foundation for the analysis of NOMA, ambient backscatter and PLS. However the joint effects of RHIs, CEEs and imperfect SIC (ipSIC) on the secure performance of the ambient backscatter NOMA systems have not yet been well investigated. To fill this gap, this paper makes an in-depth study of the joint effects of the three non-ideal factors on the reliability and the security of the ambient backscatter NOMA systems. In order to improve the security, we consider an artificial noise scheme, where the RF source sends the signal and artificial noise simultaneously. This scheme is feasible since it is carried out without changing the original system framework [34, 35]. Specifically, the analytical expressions for the OP and the intercept probability (IP) are derived for the far reader, the near reader and the tag, respectively. To obtain more insights, the asymptotic behaviors for the OP in the high signal-to-noise ratio (SNR) regime and the asymptotic behaviors for the IP in the high main-to-eavesdropper ratio (MER) region are explored. The essential contributions of this paper are summarized as follows:

- We consider a novel secure framework for the ambient backscatter NOMA systems in the presence of RHIs, CEEs, and ipSIC. To improve secure performance, an artificial noise scheme is designed.
- We derive the analytical expressions for the OP and the IP the far reader, the near reader and the tag to evaluate the reliability and the security. The results show that a smaller power coefficient of artificial noise or a larger interfering factor of readers can enhance the impact of artificial noise on balancing the trade-off reliability-security.
- In order to obtain deeper insights, we carry out the asymptotic analysis for the OP in the high SNR region as well as the diversity orders. Moreover, the asymptotic

behaviors of the IP in the high MER regime are explored by introducing the MER. The obtained results indicate that there are error floors for the OP due to the CEEs and the reflection coefficient.

B. Organization and Notations

The remainder of this paper is organised as follows. In Section II, we introduce the ambient backscatter NOMA model. In Section III, the reliability is investigated by deriving the analytical and asymptotic expressions for the OP, while the expressions of IP are derived to analyze the security. In Section IV, some numerical results are provided to validate the correctness of the theoretical analysis. Section V concludes the paper and summarizes key findings.

We use $E\{\cdot\}$ to denote the expectation operation. A complex Gaussian random variable with mean μ and variance σ^2 reads as $\mathcal{CN}\{\mu, \sigma^2\}$. $\Pr\{\cdot\}$ denotes the probability and $K_\nu(\cdot)$ represents the ν -th order modified Bessel function of the second kind, while $n!$ denotes the factorial operation. Finally, $f_X(\cdot)$ and $F_X(\cdot)$ are the probability density function (PDF) and the cumulative distribution function (CDF) of a random variable, respectively.

II. SYSTEM MODEL

As illustrated in Fig. 1, we consider a downlink ambient backscatter NOMA system, which consists of one ambient RF source (S), one tag (T), two readers (R_f , R_n) and one eavesdropper (E). In this study, S transmits the signal to readers and tag in the same resource block. Meanwhile, T transmits its own information to the readers by reflecting the signals from S signal, whereas E can intercept the signal intended for readers. We consider the following assumptions: i) All the nodes are equipped with a single antenna; ii) RHIs exist at S , readers and E but not at the tag; iii) All links h are subject to Rayleigh fading.

Under practical considerations, the perfect CSI may be unavailable due to some CEEs. The common way to obtain CSI is channel estimation. For this purpose, by adopting linear minimum mean square error (MMSE), the channel can be modeled as $h_{AB} = \hat{h}_{AB} + e_{AB}$ [36], where \hat{h}_{AB} is the estimated channel of h_{AB} , and $e_{AB} \sim \mathcal{CN}(0, \sigma_{e_{AB}}^2)$ denotes the corresponding channel estimation errors, where the variance of CEE $\sigma_{e_{AB}}^2$ indicates the quality of CSI.

To improve the security communication of ambient backscatter NOMA systems, we consider injecting artificial noise $z(t)$ with $E(|z(t)|^2) = 1$ at S . Due to the CEEs, the artificial noise will cause interference to the readers and eavesdropper. Then, the superposition message at S can be written as

$$x_s = \sqrt{a_1 P_s} x_1 + \sqrt{a_2 P_s} x_2 + \sqrt{P_J} z(t), \quad (1)$$

where P_s is the transmit power for the desired signals at S ; a_1 and a_2 are the power allocation coefficients for the near reader and the far reader with $a_1 + a_2 = 1$ and $a_1 < a_2$, respectively; x_1 and x_2 are the corresponding transmitted signals of R_n and R_f with $E(|x_1|^2) = E(|x_2|^2) = 1$; P_J is the transmitted power

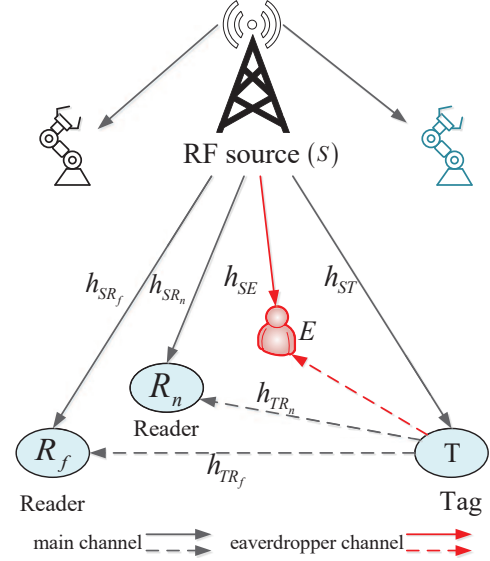


Fig. 1. Ambient backscatter NOMA system model.

of the artificial noise with $P_J = \varphi_J P_s$, with $\varphi_J \in (0, 1]$ as the power coefficient of artificial noise.

Next, T backscatters the S signal to R_f , R_n and E with its own signal $c(t)$, with $E(|c(t)|^2) = 1$. Therefore, R_f , R_n and E receive the signals from S and the backscattered from T . Considering the RHIs and CEEs, the received signals at i ($i \in \{R_f, R_n, E\}$) can be expressed as

$$y_i = \beta h_{Ti} h_{ST} (x_s c(t) + \eta_{Si}) + h_{Si} (x_s + \eta_{Si}) + n_i, \quad (2)$$

where β is a complex reflection coefficient used to normalize $c(t)$; $n_i \sim \mathcal{CN}(0, N_0)$ is the complex additive white Gaussian noise (AWGN); $\eta_{Si} \sim \mathcal{CN}(0, \kappa_{Si}^2 P_s)$; κ_{Si} denotes the level of hardware impairment at transceivers, which can be measured in practice based on the error vector magnitude (EVM) [37]; h_{Si} , h_{Ti} and h_{ST} are the channel coefficients $S \rightarrow i$, $T \rightarrow i$ and $S \rightarrow T$, respectively.

According to the NOMA protocol, R_f can decode the signals x_2 , and R_n and E can decode the signals x_2 , x_1 and $c(t)$ in turn with the aid of SIC. In addition, the readers can only eliminate part of the interference due to the presence of CEEs. Then, the received signal-to-interference-plus-noise ratio (SINR) of i ($i \in \{R_n, R_f, E\}$) can be given as²

$$\gamma_i^{x_2} = \frac{|\hat{h}_{Si}|^2 a_2 \gamma}{\gamma \left[|\hat{h}_{ST}|^2 \left(B_i |\hat{h}_{Ti}|^2 + M_i \right) + C_i |\hat{h}_{Ti}|^2 + Q_i |\hat{h}_{Si}|^2 + \psi_i \right] + 1}, \quad (3)$$

$$\gamma_i^{x_1} = \frac{|\hat{h}_{Si}|^2 a_1 \gamma}{\gamma \left[|\hat{h}_{ST}|^2 \left(B_i |\hat{h}_{Ti}|^2 + M_i \right) + C_i |\hat{h}_{Ti}|^2 + O_i |\hat{h}_{Si}|^2 + \psi_i \right] + 1}, \quad (4)$$

²It should be pointed out that R_f only needs to decode its own signal x_2 , that is, the SINR of R_f is $\gamma_{R_f}^{x_2}$.

$$\gamma_i^{c(t)} = \frac{\beta^2 |\hat{h}_{Ti}|^2 |\hat{h}_{ST}|^2 \gamma}{\gamma \left[|\hat{h}_{ST}|^2 \left(m_i |\hat{h}_{Ti}|^2 + M_i \right) + C_i |\hat{h}_{Ti}|^2 + \xi_i |\hat{h}_{Si}|^2 + \psi_i \right] + 1}, \quad (5)$$

where $\gamma = P_S/N_0$ represents the transmit SNR at S ; ε is the parameter of ipSIC; $B_{R_f} = \beta^2 (1 + \varpi \varphi_J + \kappa_{SR_f}^2)$, $C_{R_f} = B_{R_f} \sigma_{e_{ST}}^2$, $M_{R_f} = B_{R_f} \sigma_{e_{TR_f}}^2$, $Q_{R_f} = \gamma (a_1 + \varpi \varphi_J + \kappa_{SR_f}^2)$, $\psi_{R_f} = B_{R_f} \sigma_{e_{TR_f}}^2 \sigma_{e_{ST}}^2 + \sigma_{e_{SR_f}}^2 (1 + \varpi \varphi_J + \kappa_{SR_f}^2)$; ϖ is the interference factor, reflecting the degree of interference of the artificial noise to the readers, with $0 \leq \varpi \leq 1$; $B_{R_n} = \beta^2 (1 + \varpi \varphi_J + \kappa_{SR_n}^2)$, $C_{R_n} = B_{R_n} \sigma_{e_{ST}}^2$, $M_{R_n} = B_{R_n} \sigma_{e_{TR_n}}^2$, $Q_{R_n} = \gamma (a_1 + \varpi \varphi_J + \kappa_{SR_n}^2)$, $\psi_{R_n} = B_{R_n} \sigma_{e_{TR_n}}^2 \sigma_{e_{ST}}^2 + \sigma_{e_{SR_n}}^2 (1 + \varpi \varphi_J + \kappa_{SR_n}^2)$, $O_{R_n} = (\varepsilon a_2 + \varpi \varphi_J + \kappa_{SR_n}^2)$, $m_{R_n} = \beta^2 (\kappa_{SR_n}^2 + \varpi \varphi_J)$, $\xi_{R_n} = (\varepsilon + \varpi \varphi_J + \kappa_{SR_n}^2)$; $B_E = \beta^2 (1 + \varphi_J + \kappa_{SE}^2)$, $C_E = B_E \sigma_{e_{ST}}^2$, $M_E = B_E \sigma_{e_{TE}}^2$, $Q_E = \gamma (a_1 + \varphi_J + \kappa_{SE}^2)$, $\psi_E = B_E \sigma_{e_{TE}}^2 \sigma_{e_{ST}}^2 + \sigma_{e_{SE}}^2 (1 + \varphi_J + \kappa_{SE}^2)$, $O_E = (\varepsilon a_2 + \varphi_J + \kappa_{SE}^2)$, $m_E = \beta^2 (\kappa_{SE}^2 + \varphi_J)$, $\xi_E = (\varepsilon + \varphi_J + \kappa_{SE}^2)$.

III. PERFORMANCE ANALYSIS

In this section, we investigate the reliability and security of the ambient backscatter NOMA systems in term of OP and IP. In addition, the asymptotic OP and diversity orders in the high SNR regions are examined, as well as the asymptotic IP in the high MER regime.

A. OP Analysis

1) OP for R_f

The outage event occurs at R_f when R_f cannot successfully decode x_2 . Thus, the OP at R_f can be expressed as

$$P_{out}^{R_f} = 1 - \Pr \left(\gamma_{R_f}^{x_2} > \gamma_{th2}^{R_f} \right), \quad (6)$$

where $\gamma_{th2}^{R_f}$ is the target rate of R_f .

Theorem 1. For Rayleigh fading channels, the analytical expression for the OP of the far reader can be obtained as

$$P_{out}^{R_f} = 1 + \Delta_2^{R_f} e^{\Delta_1^{R_f} - \Delta_3^{R_f} - \frac{\gamma_{th2}^{R_f}}{\lambda_{SR_f} \gamma^{(a_2 - Q_{R_f} \gamma_{th2}^{R_f})}}} \text{Ei} \left(-\Delta_1^{R_f} \right), \quad (7)$$

where $\Delta_1^i = \left(\frac{M_i \gamma_{th2}^i}{\lambda_{S_i} (a_2 - Q_i \gamma_{th2}^i)} + \frac{1}{\lambda_{ST}} \right) \frac{\lambda_{S_i} (a_2 - Q_i \gamma_{th2}^i) + \lambda_{T_i} C_i \gamma_{th2}^i}{\lambda_{T_i} B_i \gamma_{th2}^i}$,

$\Delta_2^i = \frac{\lambda_{S_i} (a_2 - Q_i \gamma_{th2}^i)}{\lambda_{ST} \lambda_{T_i} B_i \gamma_{th2}^i}$, $\Delta_3^i = \frac{\psi_i \gamma_{th2}^i}{\lambda_{S_i} (a_2 - Q_i \gamma_{th2}^i)}$, ($i \in \{R_n, R_f, E\}$).

$\text{Ei}(p)$ is the exponential integral function [38] and is expressed by

$$\text{Ei}(p) = \frac{(-p)^{i-1}}{(i-1)!} [-\ln p + \psi(i)] - \sum_{m=0}^{\infty} \frac{(-p)^m}{(m-i+1)m!}, \quad (8)$$

with

$$\begin{cases} \psi(1) = -\nu \\ \psi(i) = -\nu + \sum_{m=1}^{i-1} \frac{1}{m} \quad i > 1 \end{cases}, \quad (9)$$

where $\nu \approx 0.577$ is the Euler constant.

Proof. See Appendix A. \square

Corollary 1. At high SNRs, the asymptotic expression for the OP of R_f of the ambient backscatter NOMA systems is given as

$$P_{out,\infty}^{R_f} = 1 + \Delta_2^{R_f} e^{\Delta_1^{R_f} - \Delta_3^{R_f}} \text{Ei} \left(-\Delta_1^{R_f} \right). \quad (10)$$

2) OP for R_n

To successfully decode x_1 at R_n , two conditions are needed to be met simultaneously: 1) R_n can successfully decode x_2 ; 2) R_n can successfully decode its own information x_1 . Therefore, the OP of R_n can be expressed as

$$P_{out}^{R_n} = 1 - \Pr \left(\gamma_{R_n}^{x_2} > \gamma_{th2}^{R_n}, \gamma_{R_n}^{x_1} > \gamma_{th1}^{R_n} \right), \quad (11)$$

where $\gamma_{th1}^{R_n}$ is the target rate of R_n .

Theorem 2. For Rayleigh fading channels, the analytical expression for the OP of the near reader can be obtained as

$$P_{out}^{R_n} = 1 + \frac{\lambda_{SR_n}}{\lambda_{ST} \varsigma_{R_n} \lambda_{TR_n} B_{R_n}} e^{-\left(\frac{\varsigma_{R_n}}{\lambda_{SR_n} \gamma} + \Delta_4^{R_n} \right)} \text{Ei} \left(-\Delta_4^{R_n} \right), \quad (12)$$

where $\varsigma_i = \max \left\{ \frac{\gamma_{th1}^i}{a_1 - Q_i \gamma_{th1}^i}, \frac{\gamma_{th2}^i}{a_2 - Q_i \gamma_{th2}^i} \right\}$, $\Delta_4^i = \frac{(\lambda_{ST} \varsigma_i M_i + \lambda_{S_i}) (\lambda_{S_i} + \varsigma_i \lambda_{T_i} C_i)}{\lambda_{S_i} \lambda_{ST} \varsigma_i \lambda_{T_i} B_i} + \frac{\psi_i \gamma_{th1}^i}{\lambda_{S_i}}$, ($i \in \{R_n, R_f, E\}$).

Proof. By substituting (3) and (4) into (11), we can obtain the result of (12) after some mathematical manipulations, as in the proof of **Theorem 1**. \square

Corollary 2. At high SNRs, the asymptotic expression for the OP of R_n of the ambient backscatter NOMA systems is given as

$$P_{out,\infty}^{R_n} = 1 + \frac{\lambda_{SR_n}}{\lambda_{ST} \varsigma_{R_n} \lambda_{TR_n} B_{R_n}} e^{-\left(\frac{\varsigma_{R_n} \psi_{R_n}}{\lambda_{SR_n}} + \Delta_4^{R_n} \right)} \text{Ei} \left(-\Delta_4^{R_n} \right). \quad (13)$$

3) OP for T

The T signals can be successfully decoded when x_2 and x_1 are perfectly decoded at R_n . Thus, the OP of BD can be expressed as

$$P_{out}^T = 1 - \Pr \left(\gamma_{R_n}^{x_2} > \gamma_{th2}^{R_n}, \gamma_{R_n}^{x_1} > \gamma_{th1}^{R_n}, \gamma_{R_n}^{c(t)} > \gamma_{thc}^{R_n} \right), \quad (14)$$

where γ_{thc} is the target rate for R_n decoding tag signals.

Theorem 3. For Rayleigh fading channels, we have

• Non-ideal conditions

The analytical expression for the OP of T in (15) is provided at the top of next page.

In (15), $\vartheta_k = \cos[(2k-1)\pi/(2N)]$, N is an accuracy-complexity trade-off parameter. $\Delta_5^i = \beta^2 - m_i \gamma_{thc}^i$, $\Delta_6 =$

$\left[\lambda_{TR_n} \varsigma_{R_n} C_{R_n} \gamma_{thc}^{R_n} (B_{R_n} \gamma \gamma_{thc}^{R_n} + \Delta_5) + \lambda_{SR_n} \gamma_{thc}^{R_n} \Delta_5^{R_n} \right] / (\Delta_5^{R_n} \gamma)$,

$\Delta_7^i = (\lambda_{S_i} \xi_i - \lambda_{T_i} C_i) \gamma_{thc}^i$, $\Delta_8^i = (\lambda_{T_i} C_i \gamma_{thc}^i + \Delta_7^i) \gamma$,

$A_1^i = \frac{-1}{\lambda_{S_i} \xi_i \lambda_{ST} \lambda_{T_i} \Delta_5^i \gamma^2}$, $A_2^i = -\left(\frac{C_i \gamma_{thc}^i}{\lambda_{ST} \Delta_5^i} + \frac{M_i \gamma_{thc}^i}{\lambda_{T_i} \Delta_5^i} \right)$,

$A_3^i = \frac{\lambda_{T_i} M_i (C_i \gamma \gamma_{thc}^i)^2 + (\lambda_{T_i} \psi_i \Delta_5^i + \Delta_7^i M_i) C_i \gamma^2 \gamma_{thc}^i}{\Delta_5^i} + \Delta_7^i \psi_i \gamma^2$,

$A_4^i = \lambda_{S_i}^2 \xi_i^2 \gamma_{thc}^i$, $B_1 = \frac{\lambda_{SR_n} + \lambda_{ST} \varsigma_{R_n} M_{R_n}}{\lambda_{SR_n}^2 \lambda_{ST} \lambda_{TR_n} \gamma \Delta_5^{R_n}} + \frac{\varsigma_{R_n} C_{R_n} B_{R_n} \gamma_{thc}^{R_n}}{\lambda_{SR_n}^2 \lambda_{TR_n} (\Delta_5^{R_n})^2}$,

($i \in \{R_n, R_f, E\}$), $B_5 = \frac{(\lambda_{ST} \varsigma_{R_n} C_{R_n} + \lambda_{SR_n}) C_{R_n} \gamma_{thc}^{R_n}}{\lambda_{ST} \lambda_{SR_n} \Delta_5^{R_n}} + B_2 +$

$$P_{out}^{T,ni} = 1 - \frac{2\lambda_{SR_n}}{\lambda_{TR_n}\lambda_{ST}\zeta_{R_n}B_{R_n}} e^{-\left(B_5 + \frac{\lambda_{TR_n}\zeta_{R_n}B_{R_n}\gamma_{thc}}{\lambda_{SR_n}\lambda_{TR_n}\gamma\Delta_5} + \frac{\zeta_{R_n}}{\lambda_{SR_n}\gamma}\right)} \sum_{v=1}^{\infty} (-1)^v \frac{1}{B_4^v} \left(\frac{B_3 + \Delta_6}{B_1}\right)^{\frac{v}{2}} K_v \left(2\sqrt{(B_3 + \Delta_6)B_1}\right) + \frac{\lambda_{SR_n}\xi_{R_n}\gamma_{thc}^{R_n}}{\lambda_{ST}\lambda_{TR_n}\Delta_5^{R_n}} e^{A_2^{R_n}} \left(\frac{\pi}{N} \sum_{k=0}^N e^{-\left(\frac{2(A_3^{R_n} + \Delta_8^{R_n})}{A_4^{R_n}(\vartheta_k + 1)} - \frac{A_1^{R_n}A_4^{R_n}(\vartheta_k + 1)}{2}\right)}\right) \sqrt{1 - \vartheta_k^2} \left(\frac{1}{\vartheta_k + 3} - \frac{1}{\vartheta_k + 1}\right) + 2K_0 \left(2\sqrt{-A_1^{R_n}(A_3^{R_n} + \Delta_8^{R_n})}\right). \quad (15)$$

$$B_2 = \frac{2\zeta_{R_n}B_{R_n}M_{R_n}C_{R_n}(\gamma_{thc}^{R_n})^2}{\lambda_{SR_n}(\Delta_5^{R_n})^2} + \frac{(\lambda_{BD_n}\zeta_{R_n}C_{R_n}M_{R_n} + \lambda_{SR_n}M_{R_n} + \lambda_{BR_n}\zeta_{R_n}B_{R_n}\psi_{R_n})\gamma_{thc}^{R_n}}{\lambda_{SR_n}\lambda_{BR_n}\Delta_5^{R_n}}, \quad (16)$$

$$B_3 = \left[\lambda_{TR_n}\zeta_{R_n}M_{R_n}C_{R_n}^2\gamma(\gamma_{thc}^{R_n})^2 (B_{R_n}\gamma_{thc}^{R_n} + \Delta_5^{R_n}) + (\lambda_{SR_n}M_{R_n} + \lambda_{TR_n}\zeta_{R_n}B_{R_n}\psi_{R_n})C_{R_n}\gamma(\Delta_5^{R_n}\gamma_{thc}^{R_n})^2 \right] / (\Delta_5^{R_n})^2 + (\lambda_{TR_n}\zeta_{R_n}C_{R_n} + \lambda_{SR_n})\psi_{R_n}\gamma_{thc}^{R_n}, \quad (17)$$

$$B_4 = \left[\zeta_{R_n}\lambda_{SR_n}\lambda_{BR_n}C_{R_n}\gamma(B_{R_n}\gamma_{thc}^{R_n} + \Delta_5^{R_n}) + \lambda_{SR_n}^2\Delta_5^{R_n}\gamma \right] / (\zeta_{R_n}B_{R_n}). \quad (18)$$

$\frac{\zeta_{R_n}\psi_{R_n}}{\lambda_{SR_n}}$, where B_2 , B_3 and B_4 are provided at the top of the next page.

- *Ideal conditions*

For ideal conditions, the analytical expression for the OP of the BD in (19) is provided at the top of next page.

$$\text{In (19), } \Delta_9 = \frac{\lambda_{SR_n}}{\lambda_{TR_n}\lambda_{ST}\zeta_{R_n}B_{R_n}}, \quad \Delta_{10} = \frac{(\vartheta_k + 1)\gamma_{thc}^{R_n}}{2\lambda_{TR_n}\lambda_{ST}\gamma\Delta_5^{R_n}},$$

$$\Delta_{11} = \frac{\lambda_{SR_n}\xi_{R_n}\gamma_{thc}^{R_n}}{\lambda_{TR_n}\lambda_{ST}\Delta_5^{R_n}}, \quad \text{and } \Delta_{12} = \frac{(\vartheta_k + 1)\gamma_{thc}^{R_n}}{2\lambda_{TR_n}\lambda_{ST}\gamma\Delta_5^{R_n}}.$$

Proof. See Appendix B. □

Corollary 3. At high SNRs, the asymptotic expressions for the OP of T of the ambient backscatter NOMA systems can be expressed as

- *Non-ideal conditions*

For ideal conditions, the asymptotic expression for the OP of the BD in (20) is provided at the top of next page.

- *Ideal conditions*

$$P_{out,\infty}^{T,id} = 1 + \Delta_9 e^{\Delta_9} \text{Ei}(-\Delta_9) - \Delta_{11} e^{\Delta_{11}} \text{Ei}(-\Delta_{11}). \quad (21)$$

Next, in order to obtain more insights, the diversity orders for R_f , R_n and T are investigated, which can be defined as [39]:

$$d = - \lim_{\gamma \rightarrow \infty} \frac{\log(P_{out}^{\infty})}{\log \gamma}. \quad (22)$$

Corollary 4. The diversity orders of D_f , D_n and BD are given as:

$$d_{R_f} = d_{R_n} = d_T^{id} = d_T^{ni} = 0. \quad (23)$$

Remark 1. From **Corollary 1-Corollary 4**, we can obtain that: 1) RHIs, CEEs and ipSIC have detrimental effects on the reliability of the considered systems; 2) The asymptotic outage performance of the R_f , R_n and T become a constant when the transmit SNR is in a high state, indicating that there are error floors for the OP; 3) From Eq. (23), it can be observed that the diversity orders of the considered system are zero due to the fixed constant for the OP in the high SNR regime.

B. IP Analysis

User i ($i \in \{R_f, R_n, T\}$) will be intercepted if E can successfully wiretap j 's signal, i.e., $\gamma_E^p > \gamma_{thj}^E$, $p \in \{x_2, x_1, c(t)\}$, $j \in (2, 1, c)$. Thus, the IP of i by E can be expressed as

$$P_{int}^i = \text{Pr}(\gamma_E^p > \gamma_{thj}^E), \quad (24)$$

where γ_{thj}^E is the secrecy SNR threshold of i .

Theorem 4. The analytical expressions for the IP of the far reader, the near reader and T can be respectively obtained as For the far and near readers, we have

$$P_{int}^{R_f} = -\Delta_2^E e^{\Delta_1^E - \Delta_3^E - \frac{\gamma_{th2}^E}{\lambda_{SE}\gamma(a_2 - Q_E\gamma_{th2}^E)}} \text{Ei}(-\Delta_1^E), \quad (25)$$

$$P_{int}^{R_n} = -\Delta_{16}^E e^{\Delta_{17} - \Delta_{18} - \frac{\gamma_{th2}^E}{\lambda_{SE}\gamma(a_1 - O_E\gamma_{th2}^E)}} \text{Ei}(-\Delta_{17}), \quad (26)$$

where $\Delta_{17} = \left(\frac{M_E\gamma_{th2}}{\lambda_{SE}(a_1 - O_E\gamma_{th2}^E)} + \frac{1}{\lambda_{ST}}\right) \frac{\lambda_{SE}(a_1 - O_E\gamma_{th2}^E) + \lambda_{TE}C_E\gamma_{th2}^E}{\lambda_{TE}B_E\gamma_{th2}^E}$, $\Delta_{16} = \frac{\lambda_{SE}(a_1 - O_E\gamma_{th2}^E)}{\lambda_{ST}\lambda_{TE}B_E\gamma_{th2}^E}$, and $\Delta_{18} = \frac{\psi_E\gamma_{th2}^E}{\lambda_{SE}(a_1 - O_E\gamma_{th2}^E)}$.

For T , we have

- *Non-ideal conditions*

For non-ideal conditions, the analytical expression for the IP of T in (27) is at the top of next page.

In (27), $\Delta_{13} = 1/(\lambda_{ST}\lambda_{TE}\Delta_5^E)$, $\Delta_{14} = \frac{C_E\gamma_{thc}^E(\lambda_{ST} + \lambda_{TE})}{\lambda_{TE}\lambda_{ST}\Delta_5^E}$, and $\Delta_{15} = \frac{C_E^2(\gamma_{thc}^E)^2/(\lambda_{TE}\Delta_5^E)}{\Delta_5^E} + \left(\psi_E + \frac{1}{\gamma}\right)\gamma_{thc}^E$.

- *Ideal conditions*

For ideal conditions, the analytical expression for the IP of T in (28) is at the top of next page.

Proof. See Appendix C. □

Moreover, for further investigation of the ambient backscatter NOMA secure communication systems, we also study the asymptotic behaviors of IP in the high MER region [40]. MER

$$\begin{aligned}
P_{out}^{T,id} = & 1 + \Delta_9 e^{\Delta_9 - \frac{\varsigma_{R_n}}{\lambda_{SR_n} \gamma}} \text{Ei}(-\Delta_9) + \frac{\gamma_{thc}^{R_n} \pi}{N \lambda_{TR_n} \lambda_{ST} \gamma \Delta_5^{R_n}} \sum_{k=0}^N e^{-\left(\varsigma_{R_n} B_{R_n} \Delta_{10} + \frac{\varsigma_{R_n}}{\lambda_{SR_n} \gamma}\right)} K_0\left(2\sqrt{\Delta_{10}}\right) \sqrt{1 - \vartheta_k^2} \\
& - \Delta_{11} e^{\Delta_{11} + \frac{1}{\lambda_{SR_n} \gamma \xi_{R_n}}} \text{Ei}(-\Delta_{11}) - \frac{\gamma_{thc}^{R_n} \pi}{N \lambda_{TR_n} \lambda_{ST} \gamma \Delta_5^{R_n}} \sum_{k=0}^N e^{\frac{1}{\lambda_{SR_n} \gamma \xi_{R_n}} - \frac{\vartheta_{k+1}}{2\lambda_{SR_n} \gamma \xi_{R_n}}} K_0\left(2\sqrt{\Delta_{10}}\right) \sqrt{1 - \vartheta_k^2}. \quad (19)
\end{aligned}$$

$$\begin{aligned}
P_{out,\infty}^{T,ni} = & -\frac{\lambda_{SR_n} \xi_{R_n} \gamma_{thc}^{R_n}}{\lambda_{ST} \lambda_{TD_n} \Delta_5^{R_n}} e^{A_2^{R_n}} \left(\frac{\pi}{N} \sum_{k=0}^N e^{-\left(\frac{2A_3^{R_n}}{A_4^{R_n}(\vartheta_{k+1})} - \frac{A_1^{R_n} A_4^{R_n}(\vartheta_{k+1})}{2}\right)} \sqrt{1 - \vartheta_k^2} \left(\frac{1}{\vartheta_{k+3}} + \frac{1}{\vartheta_{k+1}} \right) - 2K_0\left(2\sqrt{-A_1^{R_n} A_3^{R_n}}\right) \right) \\
& + \frac{2\lambda_{SR_n}}{\lambda_{TR_n} \lambda_{ST} \varsigma_{R_n} B_{R_n}} e^{-B_5} \sum_{v=1}^{\infty} (-1)^v \frac{1}{B_4^v} \left(\frac{B_3}{B_1} \right)^{\frac{v}{2}} K_v\left(2\sqrt{B_3 B_1}\right). \quad (20)
\end{aligned}$$

$$\begin{aligned}
P_{int}^{T,ni} = & -\frac{\lambda_{SE} \xi_E \gamma_{thc}^E}{\lambda_{ST} \lambda_{TE} \Delta_5^E} e^{A_2^E} \left(\frac{\pi}{N} \sum_{k=0}^N e^{-\left(\frac{2(A_3^E + \Delta_8^E)}{A_4^E(\vartheta_{k+1})} - \frac{A_1^E A_4^E(\vartheta_{k+1})}{2}\right)} \sqrt{1 - \vartheta_k^2} \left(\frac{1}{\vartheta_{k+3}} - \frac{1}{\vartheta_{k+1}} \right) + 2K_0\left(2\sqrt{-A_1^E (A_3^E + \Delta_8^E)}\right) \right) \\
& + 2\sqrt{\Delta_{15} \Delta_{13}} e^{-\Delta_{14}} K_1\left(2\sqrt{\Delta_{13} \Delta_{15}}\right). \quad (27)
\end{aligned}$$

TABLE I
TABLE OF PARAMETERS FOR NUMERICAL RESULTS.

Power sharing coefficients of NOMA	$a_1 = 0.2, a_2 = 0.8$
Noise power	$N_0 = 1$
Reflection coefficient	$\beta = 0.1$
ipSIC parameter	$\varepsilon = 0.01$
Power coefficient of artificial noise	$\varphi_J = 0.1$
Interfering factor of readers	$\varpi = 0.5$
RHIs parameter	$\kappa_{SR_f} = \kappa_{SR_n} = \kappa_{SE} = \kappa = 0.1$
Channel fading parameters	$\{\lambda_{SR_f}, \lambda_{SR_n}, \lambda_{SB}, \lambda_{SE}, \lambda_{TR_f}, \lambda_{TR_n}, \lambda_{TE}\} = \{4, 6, 1, 0.5, 1, 2, 0.3\}$
CEEs parameter	$\sigma_{eSR_f}^2 = \sigma_{eSR_n}^2 = \sigma_{eSB}^2 = \sigma_{eSE}^2 = \sigma_{eTR_f}^2 = \sigma_{eTR_n}^2 = \sigma_{eTE}^2 = \sigma_e^2 = 0.05$
Targeted data rates (OP)	$\{\gamma_{th1}^{R_n}, \gamma_{th2}^{R_n} = \gamma_{th2}^{R_f}, \gamma_{thc}^{R_n}\} = \{1.2, 1, 0.001\}$
Targeted data rates (IP)	$\{\gamma_{th1}^E, \gamma_{th2}^E, \gamma_{thc}^E\} = \{0.12, 0.3, 0.01\}$

$$\begin{aligned}
P_{int}^{T,id} = & 1 - \frac{\pi \gamma_{thc}^E}{N \lambda_{ST} \lambda_{TE} \gamma \Delta_5^E} \sum_{k=0}^N (\vartheta_{k+1}) K_0\left((\vartheta_{k+1}) \sqrt{\frac{\gamma_{thc}^E}{\lambda_{ST} \lambda_{TE} \gamma \Delta_5^E}}\right) \sqrt{1 - \vartheta_k^2} \\
& - \frac{2}{\lambda_{ST} \lambda_{TE}} e^{\frac{1}{\lambda_{SE} \xi_E \gamma}} \int_{\frac{\gamma_{thc}^E}{\Delta_5^E}}^{\infty} e^{-\frac{\Delta_8^E y}{\lambda_{SE} \xi_E \gamma_{thc}^E}} K_0\left(2\sqrt{\frac{y}{\lambda_{ST} \lambda_{TE}}}\right) dy. \quad (28)
\end{aligned}$$

is introduced to distinguish the channel state of the main link and eavesdropping link, being defined as $\lambda_{me} = \frac{\lambda_{ST}}{\lambda_{TE}}$.

Corollary 5. *At high MERs, the asymptotic expression for the IP of R_f of the ambient backscatter NOMA systems is given as*

$$P_{int,\infty}^{R_f} = -\Delta_2' e^{\Delta_1' - \Delta_3' - \frac{\gamma_{th2}^E}{\lambda_{SE} \gamma (a_2 - Q_E \gamma_{th2}^E)}} (1 + b_1') \text{Ei}(-(\Delta_1' + b_1')), \quad (29)$$

$$\begin{aligned}
\text{where } \Delta_1' = & \frac{M_E}{\lambda_{TE} B_E} + \frac{M_E C_E \gamma_{th2}^E}{\lambda_{SE} (a_2 - Q_E \gamma_{th2}^E) B_E}, \quad \Delta_2' = \frac{\lambda_{SE} (a_2 - Q_E \gamma_{th2}^E)}{\lambda_{me} \lambda_{TE} B_E \gamma_{th2}^E}, \\
\Delta_3' = & \frac{\psi_E \gamma_{th2}^E}{\lambda_{SE} (a_2 - Q_E \gamma_{th2}^E)}, \quad \text{and } b_1' = \frac{\lambda_{SE} (a_2 - Q_E \gamma_{th2}^E) + \lambda_{TE} C_E \gamma_{th2}^E}{\lambda_{me} \lambda_{TE}^2 B_E \gamma_{th2}^E}.
\end{aligned}$$

Proof. The proof follows by taking λ_{me} large in (29) and simplifying the expressions by utilizing $e^x \approx 1 + x$ if $x \rightarrow 0$. Similarly, we can also obtain (30). \square

Corollary 6. *At high MERs, the asymptotic expression for the IP of R_n of the ambient backscatter NOMA systems is given as*

$$\begin{aligned}
P_{int,\infty}^{R_n} = & -\Delta_{16}' e^{\Delta_{17}' - \Delta_{18}' - \frac{\gamma_{th2}^E}{\lambda_{SE} \gamma (a_1 - O_E \gamma_{th2}^E)}} \\
& \times (1 + b_2') \text{Ei}(-(\Delta_{17}' + b_2')), \quad (30)
\end{aligned}$$

$$\text{where } \Delta_{17}' = \frac{M_E}{\lambda_{TE} B_E} + \frac{M_E C_E \gamma_{th2}^E}{\lambda_{SE} (a_1 - O_E \gamma_{th2}^E) B_E}, \Delta_{16}' = \frac{\lambda_{SE} (a_1 - O_E \gamma_{th2}^E)}{\lambda_{me} \lambda_{TE}^2 B_E \gamma_{th2}^E},$$

$$\Delta_{18}' = \frac{\psi^E \gamma_{th2}^E}{\lambda_{SE} (a_1 - Q_E \gamma_{th2}^E)}, \text{ and } b_2' = \frac{\lambda_{SE} (a_1 - O_E \gamma_{th2}^E) + \lambda_{TE} C_E \gamma_{th2}^E}{\lambda_{me} \lambda_{TE}^2 B_E \gamma_{th2}^E}.$$

Corollary 7. *At high MERs, the asymptotic expression for the IP of T of the ambient backscatter NOMA systems can be written by*

- *Non-ideal conditions*

For non-ideal conditions, the asymptotic expression for the OP of the BD in (31) is provided at the top of next page.

$$\text{In (31), } A_1' = -\frac{1}{\lambda_{SE} \xi_E \lambda_{me} \lambda_{TE}^2 \Delta_5^E \gamma^2}, \Delta_{13}' = \frac{1}{\lambda_{me} \lambda_{TE}^2 \Delta_5^E},$$

$$K_1 \left(2\sqrt{\Delta_{13}' \Delta_{15}'} \right) \approx I_1 \left(2\sqrt{\Delta_{13}' \Delta_{15}'} \right) \left(\ln \left(\sqrt{\Delta_{13}' \Delta_{15}'} \right) + \nu \right) +$$

$$\frac{1}{2} \left(\sqrt{\Delta_{13}' \Delta_{15}'} \right)^{-1} - \frac{1}{2} \sum_{l=0}^3 \frac{\left(\sqrt{\Delta_{13}' \Delta_{15}'} \right)^{2l+1}}{l!(l+1)} \left(\sum_{k=1}^l \frac{1}{k} + \sum_{k=1}^{l+1} \frac{1}{k} \right).$$

- *Ideal conditions*

For Ideal conditions, the analytical expression for the IP of T in (32) is provided at the top of next page.

Proof. The proof follows by taking λ_{me} large in (31) and (32) and simplifying the expressions by utilizing $e^{-x} \approx 1 - x$ and $K_0(x) \approx -\ln(x)$ if $x \rightarrow 0$. \square

Remark 2. *From Theorem 4 and Corollary 5-Corollary 7, the following observations can be inferred: 1) RHIs, CEEs and ipSIC can enhance the security of the ambient backscatter NOMA systems; 2) When the reflection coefficient β increases, both $P_{int}^{R_f}$ and $P_{int}^{R_n}$ decrease, while P_{int}^T increases; 3) Increasing φ_J can reduce the IP, thereby improving the reliability-security trade-off of the considered systems; 4) as λ_{me} grows, the security for R_n and R_f is improved, while the security for T is reduced.*

IV. NUMERICAL RESULTS

In this section, simulation results are provided to verify the correctness of our theoretical analysis in Section III. The results are verified by using Monte Carlo simulations with 10^6 trials. Unless otherwise stated, we set the parameters as shown in Table I is at the top of the previous page.

Fig. 2 plots the OP and the IP versus the transmit SNR for the far reader, the near reader and T, with $\kappa = 0.1$ and $\sigma_e^2 = 0.05$. For comparison, the considered system performance of ideal conditions is provided with $\kappa = 0$ and $\sigma_e^2 = 0$. It is shown that the theoretical results match well the simulations across the entire SNR region. We can also observe that the OP approaches a fixed constant due to the fixed estimation error and β in the high SNR region, which results in zero diversity order. These results verify the conclusion in **Remark 1**. Moreover, RHIs have a positive impact on IP, which reveals that the ideal communication systems are more vulnerable to be eavesdropped than the non-ideal communication systems. Finally, we can also see that there exists a trade-off between reliability and security.

Fig. 3 demonstrates the impact of OP versus IP for different power coefficient of the artificial noise φ_J and attenuation factor ϖ , with $\varphi_J = \{0.1, 0.4\}$ and $\varpi = \{0.2, 0.05\}$. In this simulation, we assume $\kappa = 0$ and $\sigma_e^2 = 0$. One can observe

that as the power coefficient of the artificial noise φ_J grows smaller, the reliability-security tradeoff of the considered system degrades significantly. This is because the interference signals at eavesdropper become more dominant, resulting in a higher IP. Similarly, the interference factor ϖ of the readers increases so as to result in a higher OP, which indicates that the reliability-security tradeoff degrades obviously. It is noted that the IP of T is the smallest, implying that T has the most secure performance. Therefore, in order to improve reliability-security tradeoff of the system by artificial noise, the design with a greater power coefficient of the artificial noise and smaller interference factor of the reader is more important.

Fig. 4 presents the OPs and IPs versus RHIs κ and CEEs σ_e^2 . In this simulation, we set SNR = 25 dB and $\varphi_J^{R_n} = 0.05$ for the OP, while SNR = 5 dB and $\varphi_J^E = 0.2$ for IP. According to Fig.4 (a) and (b), it is clear that as κ grows, $P_{out}^{R_f}$, $P_{out}^{R_n}$ and P_{out}^T increase, while $P_{int}^{R_f}$, $P_{int}^{R_n}$ and P_{int}^T decrease. Likewise, with an increasing σ_e^2 , the OPs of R_f , R_n and T increase, whereas those of the corresponding IPs decrease. It means that the reliability of T is the worst, while it has better security. Moreover, for R_f , R_n and T , the fluctuation for the OP and IP of RHIs is more obvious than that of CEEs, which shows that the reliability and security of the readers are more dependent on the ability of RHIs. Finally, we can also observe that as RHIs change, the OP of far reader changes drastically. In contrast, the change of OP of T is the least obvious, most probably because T eliminate part of interference caused by the far and near readers.

Fig. 5 illustrates the OP and IP versus the transmit SNR for different ε and β , respectively. In this simulation, we set: $\varepsilon = \{0, 0.05\}$, $\beta = \{0.2, 0.12\}$ for OP; $\varepsilon = \{0, 0.3\}$, $\beta = \{0.1, 0.3\}$ for IP. As can be seen in Fig. 5 (a), the error floors for the OP happen at high transmit SNR. The OP decreases as the transmit SNR increases, and depends on the value of ε and β . More specifically, under perfect SIC ($\varepsilon = 0$), the outage behaviors of R_f , R_n and T improve remarkably when β increases; similarly, for a fixed β , the increase of ε also leads to lower reliability of R_n and T . By comparing Fig. 5 (a) with 5 (b), we can observe that ε and β have opposite effects on IP for the far reader, near reader, and T , while β has identical effects on T, i.e., the increase of β reduces the security of T . It is worth noting that OPs of R_f and R_n are more sensitive to β , which is due to the increase of interference from the backscatter link. For IP, T is more sensitive to β . This happens because when β increases, E is more likely to eavesdrop the information of $c(t)$ successfully.

Fig. 6 presents the IP versus MER for R_f , R_n , and T under ideal conditions with $\kappa = 0$, $\sigma_e^2 = 0$, as well as non-ideal conditions with $\kappa = 0.1$, $\sigma_e^2 = 0.05$. In this simulation, we set SNR = 5 dB, $\lambda_{TE} = 2$, and $\{\gamma_{th1}^E, \gamma_{th2}^E, \gamma_{thc}^E\} = \{0.3, 0.3, 1\}$. From Fig. 6, we can observe that the asymptotic results are strict approximation of the IP in the high MER regime and the RHIs can enhance the security of R_f , R_n , and T . In addition, the IP of R_f is much larger than that of R_n when R_f and R_n have the same target rate, which is due to the fact that R_f allocates more power. Therefore, considering the small power allocation coefficients a_1 and high target rate γ_{th1}^E of the R_n ,

³For large MER, in order to achieve a better approximation effect, we only need to consider the first three terms of l , i.e. $l = 1, 2, 3$.

$$\begin{aligned}
P_{int,\infty}^{T,ni} = & -\frac{\pi\lambda_{SE}\xi_E\gamma_{thc}^E}{N\lambda_{me}\lambda_{TE}^2\Delta_5^E} e^{-\frac{M_E\gamma_{thc}^E}{\lambda_{TE}\Delta_5^E}} \left(1 - \frac{C_E\gamma_{thc}^E}{\lambda_{me}\lambda_{TE}\Delta_5^E}\right) \sum_{k=0}^N e^{-\frac{2(A_3^E+\Delta_8^E)}{A_4^E(\vartheta_k+1)}} \left(1 + \frac{A_1'A_4^E(\vartheta_k+1)}{2}\right) \sqrt{1-\vartheta_k^2} \left(\frac{1}{\vartheta_k+3} - \frac{1}{\vartheta_k+1}\right) \\
& + \frac{\lambda_{SE}\xi_E\gamma_{thc}^E}{\lambda_{me}\lambda_{TE}^2\Delta_5^E} e^{-\frac{M_E\gamma_{thc}^E}{\lambda_{TE}\Delta_5^E}} \left(1 - \frac{C_E\gamma_{thc}^E}{\lambda_{me}\lambda_{TE}\Delta_5^E}\right) \ln\left(\sqrt{-A_1^E(A_3^E+\Delta_8^E)} + 2\sqrt{\Delta_{15}\Delta_{13}'}K_1\left(2\sqrt{\Delta_{13}'\Delta_{15}}\right)\right) e^{-\frac{C_E\gamma_{thc}^E}{\lambda_{TE}\Delta_5^E}} \left(1 - \frac{C_E\gamma_{thc}^E}{\lambda_{me}\lambda_{TE}\Delta_5^E}\right). \tag{31}
\end{aligned}$$

$$\begin{aligned}
P_{int,\infty}^{T,id} = & 1 + \frac{\pi\gamma_{thc}^E}{N\lambda_{me}\lambda_{TE}^2\gamma\Delta_5^E} \sum_{k=0}^N (\vartheta_k+1) \ln\left(\frac{\vartheta_k+1}{2} \sqrt{\frac{\gamma_{thc}^E}{\lambda_{me}\lambda_{TE}^2\gamma\Delta_5^E}}\right) \sqrt{1-\vartheta_k^2} \\
& + \frac{2}{\lambda_{me}\lambda_{TE}^2} e^{\frac{1}{\lambda_{SE}\xi_E\gamma}} \int_{\frac{\gamma_{thc}^E}{\Delta_5^E}}^{\infty} e^{-\frac{\Delta_5^E y}{\lambda_{SE}\xi_E\gamma_{thc}^E}} \ln\left(\sqrt{\frac{y}{\lambda_{me}\lambda_{TE}^2}}\right) dy. \tag{32}
\end{aligned}$$

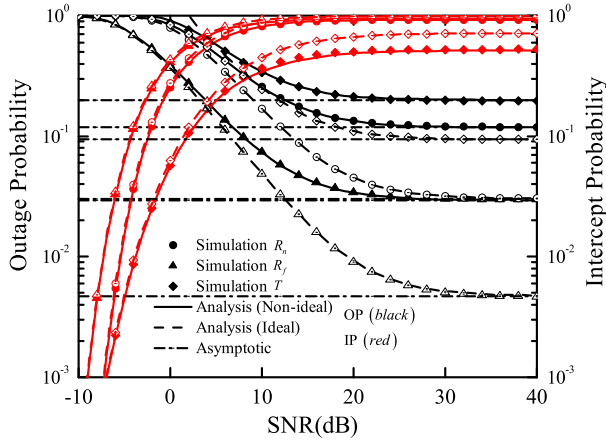
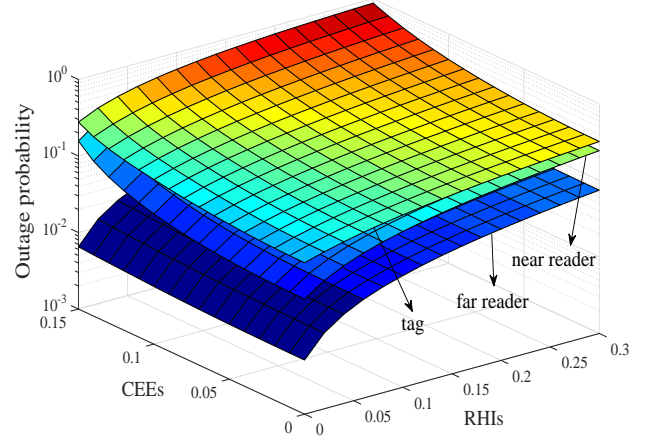
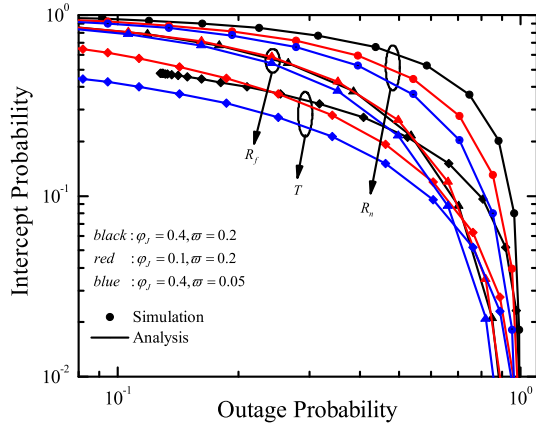
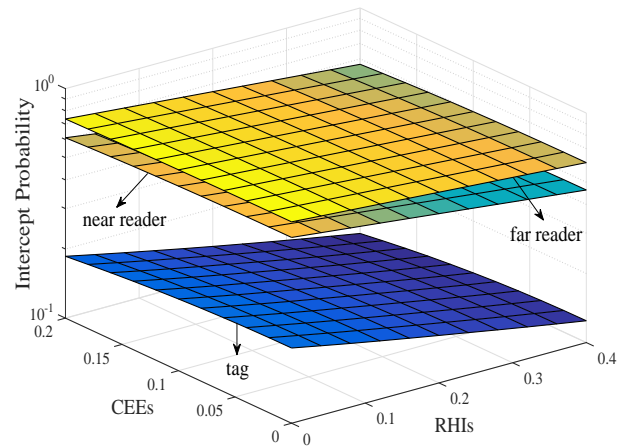


Fig. 2. OP and IP versus the transmit SNR.



(a) OP versus RHI and CEEs.

Fig. 3. IP versus OP for different power coefficient of artificial noise φ_j .

(b) IP versus RHI and CEEs.

Fig. 4. OP and IP versus RHI and CEEs.

it is difficult for the information of R_n to be eavesdropped by E . Finally, we can also observe that as MER grows, the security for R_n and R_f is improved, while the security for T

is reduced.

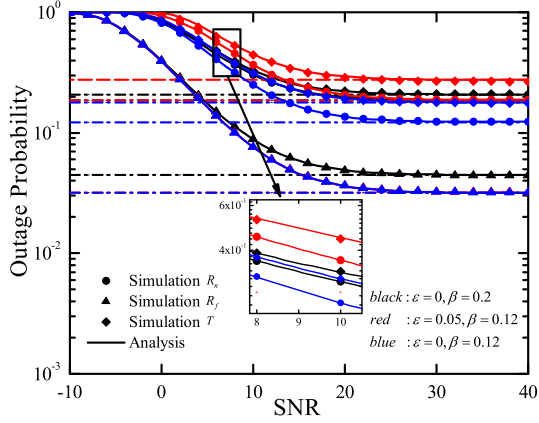
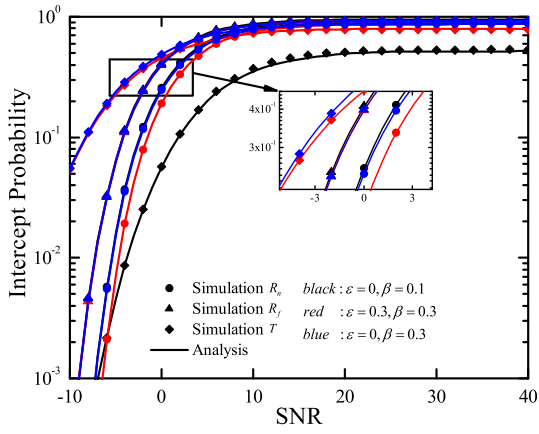
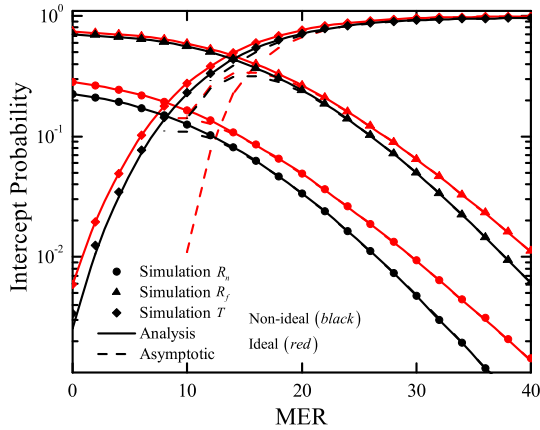
(a) OP versus the transmit SNR for different ε and β .(b) IP versus the transmit SNR for different ε and β .Fig. 5. OP and IP versus the transmit SNR for different ε and β .

Fig. 6. IP versus MER for ideal and non-ideal conditions.

V. CONCLUSION

In this paper, we investigate the joint impacts of RHIs, CEEs and ipSIC on the reliability and the security of the

ambient backscatter NOMA systems in terms of OP and IP. To improve the security performance, an artificial noise scheme was proposed, where the RF source simultaneously sends the signal and artificial noise to the readers and tag. The analytical expressions for the OP and the IP were derived. Furthermore, the asymptotic OP in the high SNR regime and the asymptotic IP in the high MER region are analyzed. The simulation results show that although RHIs, CEEs and ipSIC all have a significant negative impact for the OP of the far reader, near reader, and tag, they have a obvious positive effect for the IP on the three devices. In addition, the increase of β will reduce the reliability and enhance the security for far reader and near reader. Finally, we can conclude that the optimal reliability-security tradeoff performance can be achieved by adjusting the power coefficient of the artificial noise and interference factor of the reader, which further drives ambient backscatter application in the IoT networks.

APPENDIX A: PROOF OF THEOREM 1

Substituting (3) into (6), the OP of R_f can be expressed as

$$P_{out}^{R_f} = 1 - \underbrace{\Pr(\gamma_{R_f}^{x_2} > \gamma_{th2}^{R_f})}_{I_1}, \quad (\text{A.1})$$

where I_1 is calculated as follows:

$$\begin{aligned} I_1 &= \Pr(\gamma_{R_f}^{x_2} > \gamma_{th2}^{R_f}) \\ &= \int_{\alpha_1}^{\infty} \frac{1}{\lambda_{SR_f}} e^{-\frac{x}{\lambda_{SD_f}}} \frac{1}{\lambda_{TR_f}} e^{-\frac{y}{\lambda_{TR_f}}} \frac{1}{\lambda_{ST}} e^{-\frac{z}{\lambda_{ST}}} dx dy dz \\ &= \int_{\alpha}^{\infty} e^{-\alpha_3 u} \frac{1}{u} du \\ &\stackrel{l_1}{=} 1 + \Delta_2^{R_f} e^{\Delta_1^{R_f} - \Delta_3^{R_f} - \frac{\gamma_{th2}^{R_f}}{\lambda_{SR_f} \gamma_{(a_2 - Q_{R_f} \gamma_{th2}^{R_f})}}} \text{Ei}(-\Delta_1^{R_f}), \quad (\text{A.2}) \end{aligned}$$

where $\alpha_1 = \frac{(B_{R_f} z + C_{R_f}) \gamma_{th2}^{R_f} y + M_{R_f} \gamma_{th2}^{R_f} z + (\psi_{R_f} + 1) \gamma_{th2}^{R_f}}{(a_2 - Q_{R_f} \gamma_{th2}^{R_f}) \gamma}$, $\alpha_2 = \frac{\lambda_{SR_f} (a_2 - Q_{R_f} \gamma_{th2}^{R_f}) + \lambda_{TR_f} C_{R_f} \gamma_{th2}^{R_f}}{\lambda_{TR_f} B_{R_f} \gamma_{th2}^{R_f}}$, $\alpha_3 = \frac{M_{R_f} \gamma_{th2}^{R_f}}{\lambda_{SR_f} (a_2 - Q_{R_f} \gamma_{th2}^{R_f})} + \frac{1}{\lambda_{ST}}$, and the step l_1 is obtained by utilizing [41, Eq. (3.352)]. Finally, substituting (A.2) into (A.1), we can obtain (7).

Similarly, substituting (3) and (4) into (11), the (12) can be obtained.

APPENDIX B: PROOF OF THEOREM 3

Substituting (3), (4) and (5) into (14), the OP of T can be expressed as

$$P_{out}^T = 1 - \underbrace{\Pr(\gamma_{R_n}^{x_2} > \gamma_{th2}^{R_n}, \gamma_{R_n}^{x_1} > \gamma_{th1}^{R_n}, \gamma_{R_n}^{c(t)} > \gamma_{thc}^{R_n})}_{I_2}, \quad (\text{B.1})$$

• Non-ideal conditions

For non-ideal conditions, I_2 is calculated as (A.2), shown at the top of the next page.

$$\begin{aligned}
I_2 &= \text{Pr} \left(\varsigma_{R_n} \gamma \left[\left(B_{R_n} |\hat{h}_{ST}|^2 + C_{R_n} \right) |\hat{h}_{TR_n}|^2 + M_{R_n} |\hat{h}_{ST}|^2 + \psi_{R_n} + \frac{1}{\gamma} \right] < |\hat{h}_{SR_n}|^2 < \frac{\left(\Delta_5^{R_n} |\hat{h}_{ST}|^2 - C_{R_n} \gamma_{thc}^{R_n} \right) |\hat{h}_{TR_n}|^2 - M_{R_n} |\hat{h}_{ST}|^2 \gamma_{thc}^{R_n} - \left(N_{R_n} + \frac{1}{\gamma} \right) \gamma_{thc}^{R_n}}{\xi_{R_n} \gamma_{thc}^{R_n}} \right) \\
&= \int_{\frac{C_{R_n} \gamma_{thc}^{R_n}}{\Delta_5^{R_n}}}^{\infty} \int_{\frac{M_{R_n} \gamma_{thc}^{R_n} z + (\psi_{R_n} + \frac{1}{\gamma}) \gamma_{thc}^{R_n}}{\Delta_5^{R_n} z - C_{R_n} \gamma_{thc}^{R_n}}}^{\infty} \int_{\varsigma_{R_n} \left[(B_{R_n} z + C_{R_n}) y + M_{R_n} z + \psi_{R_n} + \frac{1}{\gamma} \right]}^{\frac{(\Delta_5^{R_n} z - C_{R_n} \gamma_{thc}^{R_n}) y - M_{R_n} \gamma_{thc}^{R_n} z - (\psi_{R_n} + \frac{1}{\gamma}) \gamma_{thc}^{R_n}}{\xi_{R_n} \gamma_{thc}^{R_n}}}^{\infty} \frac{1}{\lambda_{SR_n}} e^{-\frac{x}{\lambda_{SR_n}}} \frac{1}{\lambda_{TR_n}} e^{-\frac{y}{\lambda_{TR_n}}} \frac{1}{\lambda_{ST}} e^{-\frac{z}{\lambda_{ST}}} dx dy dz \\
&= \underbrace{\int_{\frac{C_{R_n} \gamma_{thc}^{R_n}}{\Delta_5^{R_n}}}^{\infty} \int_{\frac{M_{R_n} \gamma_{thc}^{R_n} z + (\psi_{R_n} + \frac{1}{\gamma}) \gamma_{thc}^{R_n}}{\Delta_5^{R_n} z - C_{R_n} \gamma_{thc}^{R_n}}}^{\infty} e^{-\frac{1}{\lambda_{SR_n}} \varsigma_{R_n} \left[(B_{R_n} z + C_{R_n}) y + M_{R_n} z + \psi_{R_n} + \frac{1}{\gamma} \right]} \frac{1}{\lambda_{TR_n}} e^{-\frac{y}{\lambda_{TR_n}}} \frac{1}{\lambda_{ST}} e^{-\frac{z}{\lambda_{ST}}} dy dz}_{I_{21}} \\
&\quad - \underbrace{\int_{\frac{C_{R_n} \gamma_{thc}^{R_n}}{\Delta_5^{R_n}}}^{\infty} \int_{\frac{M_{R_n} \gamma_{thc}^{R_n} z + (\psi_{R_n} + \frac{1}{\gamma}) \gamma_{thc}^{R_n}}{\Delta_5^{R_n} z - C_{R_n} \gamma_{thc}^{R_n}}}^{\infty} e^{-\frac{(\Delta_5^{R_n} z - C_{R_n} \gamma_{thc}^{R_n}) y - M_{R_n} \gamma_{thc}^{R_n} z - (\psi_{R_n} + \frac{1}{\gamma}) \gamma_{thc}^{R_n}}{\lambda_{SR_n} \xi_{R_n} \gamma_{thc}^{R_n}}} \frac{1}{\lambda_{TR_n}} e^{-\frac{y}{\lambda_{TR_n}}} \frac{1}{\lambda_{ST}} e^{-\frac{z}{\lambda_{ST}}} dy dz}_{I_{22}}. \quad (\text{B.2})
\end{aligned}$$

By using some mathematical manipulations, we can obtain

$$\begin{aligned}
I_{21} &= \int_{\frac{C_{R_n} \gamma_{thc}^{R_n}}{\Delta_5^{R_n}}}^{\infty} \alpha_5 e^{-\frac{\varsigma_{R_n} (M_{R_n} z + \psi_{R_n} + \frac{1}{\gamma})}{\lambda_{SR_n}} - \alpha_4} \frac{1}{\lambda_{ST}} e^{-\frac{z}{\lambda_{ST}}} dz \\
&= \int_0^{\infty} \frac{\lambda_{SR_n}}{\lambda_{TR_n} \lambda_{ST} \varsigma_{R_n} B_{R_n}} e^{-\alpha_6} \frac{1}{u + B_4} e^{-(B_1 u + \frac{B_3 + \Delta_6}{u})} du \\
&= \frac{\lambda_{SR_n}}{\lambda_{TR_n} \lambda_{ST} \varsigma_{R_n}} e^{-B_6} \sum_{v=1}^{\infty} (-1)^v \frac{1}{B_4^v} \int_0^{\infty} u^{v-1} e^{-(B_1 u + \frac{B_3 + \Delta_6}{u})} du \\
&= \frac{l_2}{\lambda_{TR_n} \lambda_{ST} \varsigma_{R_n} B_{R_n}} e^{-\alpha_6} \sum_{v=1}^{\infty} (-1)^v \frac{1}{B_4^v} \left(\frac{B_3 + \Delta_6}{B_1} \right)^{\frac{v}{2}} K_v \left(2\sqrt{(B_3 + \Delta_6) B_1} \right), \quad (\text{B.3})
\end{aligned}$$

where $u = \lambda_{SR_n} \lambda_{TR_n} \Delta_5^{R_n} z - \lambda_{SR_n} \lambda_{TR_n} C_{R_n} \gamma_{thc}^{R_n}$, $\alpha_4 = \frac{[\lambda_{TR_n} \varsigma_{R_n} (B_{R_n} z + C_{R_n}) + \lambda_{SR_n} (\psi_{R_n} + \frac{1}{\gamma}) \gamma_{thc}^{R_n} + M_{R_n} \gamma_{thc}^{R_n} z]}{\lambda_{SR_n} \lambda_{TR_n} (\Delta_5^{R_n} z - C_{R_n} \gamma_{thc}^{R_n})}$, $\alpha_5 = \frac{\lambda_{SR_n}}{\lambda_{TR_n} \varsigma_{R_n} (B_{R_n} z + C_{R_n}) + \lambda_{SR_n}}$, $\alpha_6 = B_5 + \frac{\lambda_{TR_n} \varsigma_{R_n} B_{R_n} \gamma_{thc}^{R_n}}{\lambda_{SR_n} \lambda_{TR_n} \gamma_{thc}^{R_n}} + \frac{\varsigma_{R_n}}{\lambda_{SR_n} \gamma}$, and l_2 is obtained by utilizing [14, Eq. (3.471)].

$$\begin{aligned}
I_{22} &= \int_{\frac{C_{R_n} \gamma_{thc}^{R_n}}{\Delta_5^{R_n}}}^{\infty} \frac{e^{\frac{\psi_{R_n} + \frac{1}{\gamma}}{\lambda_{SR_n} \xi_{R_n}} + \left(\frac{M_{R_n}}{\lambda_{SR_n} \xi_{R_n}} - \frac{1}{\lambda_{ST}} \right) z - \alpha_7} \lambda_{SR_n} \xi_{R_n} \gamma_{thc}^{R_n}}{\lambda_{ST} (\lambda_{TR_n} \Delta_5^{R_n} z + \Delta_7^{R_n})} dz \\
&= \frac{\lambda_{SR_n} \xi_{R_n} \gamma_{thc}^{R_n}}{\lambda_{ST} \lambda_{TR_n} \Delta_5^{R_n}} e^{A_2^{R_n}} \int_0^{\infty} e^{-\left((-A_1^{R_n}) u + \frac{A_3^{R_n} + \Delta_8^{R_n}}{u} \right)} \frac{1}{u + A_4^{R_n}} du \\
&= \frac{\lambda_{SR_n} \xi_{R_n} \gamma_{thc}^{R_n}}{\lambda_{ST} \lambda_{TR_n} \Delta_5^{R_n}} e^{A_2^{R_n}} \left[\underbrace{\int_0^{A_4^{R_n}} e^{-\left((-A_5) u + \frac{A_3}{u} \right)} \frac{1}{u + A_4^{R_n}} du}_{l_3} \right. \\
&\quad \left. + \underbrace{\int_{A_4^{R_n}}^{\infty} e^{-\left((-A_1^{R_n}) u + \frac{A_3^{R_n} + \Delta_8^{R_n}}{u} \right)} \frac{1}{u + A_4^{R_n}} du}_{l_4} \right], \quad (\text{B.4})
\end{aligned}$$

where $u = \lambda_{SR_n} \xi_{R_n} \lambda_{TR_n} \Delta_5^{R_n} z - \lambda_{SR_n} \xi_{R_n} \lambda_{TR_n} C_{R_n} \gamma_{thc}^{R_n}$, $\alpha_7 = \frac{(\lambda_{TR_n} \Delta_5^{R_n} z + \Delta_7^{R_n}) (\psi_{R_n} + \frac{1}{\gamma} + M_{R_n} z)}{\lambda_{SR_n} \xi_{R_n} \lambda_{TR_n} [\Delta_5^{R_n} z - C_{R_n} \gamma_{thc}^{R_n}]}$, and

l_3 can be approximated by the Gaussian-Chebyshev quadrature [42], i.e., $l_3 \approx \frac{\pi}{N} \sum_{k=0}^N \frac{1}{(\vartheta_k + 3)} e^{-\left(\frac{2(A_3^{R_n} + \Delta_8^{R_n})}{A_4^{R_n} (\vartheta_k + 1)} - \frac{A_1^{R_n} A_4^{R_n} (\vartheta_k + 1)}{2} \right)} \sqrt{1 - \vartheta_k^2}$.

Next, due to $A_4^{R_n} \leq 1$, l_4 can be expressed as

$$\begin{aligned}
l_4 &\approx \int_{A_4^{R_n}}^{\infty} e^{-\left((-A_1^{R_n}) u + \frac{A_3^{R_n} + \Delta_8^{R_n}}{u} \right)} \frac{1}{u} du \\
&= \int_0^{\infty} e^{-\left((-A_1^{R_n}) u + \frac{A_3^{R_n} + \Delta_8^{R_n}}{u} \right)} \frac{1}{u} du \\
&\quad - \int_0^{A_4^{R_n}} e^{-\left((-A_1^{R_n}) u + \frac{A_3^{R_n} + \Delta_8^{R_n}}{u} \right)} \frac{1}{u} du \\
&= 2K_0 \left(2\sqrt{-A_1^{R_n} (A_3^{R_n} + \Delta_8^{R_n})} \right) - \\
&\quad \frac{\pi}{N} \sum_{k=0}^N \frac{1}{\vartheta_k + 1} e^{-\left(\frac{2(A_3^{R_n} + \Delta_8^{R_n})}{A_4^{R_n} (\vartheta_k + 1)} - \frac{A_1^{R_n} A_4^{R_n} (\vartheta_k + 1)}{2} \right)} \sqrt{1 - \vartheta_k^2}. \quad (\text{B.5})
\end{aligned}$$

By substituting l_3 and (B.5) into (B.4), I_{22} can be obtained; substituting (B.3) and (B.4) into (B.2), I_2 can be derived.

• Ideal conditions

Substituting $\kappa = 0$ and $\sigma_e^2 = 0$ into (3), (4) and (5), $C_{R_f} = M_{R_f} = C_{R_n} = M_{R_n} = 0$. Then, the OP of T under ideal conditions is given at the top of next page.

In (B.6), I_{31} can be obtained by utilizing [41, Eq. (6.611)], I_{32} can be approximated by the Gaussian-Chebyshev quadrature [42]. Thus, I_{31} and I_{32} can be expressed as

$$I_{31} = \Delta_{11} e^{\Delta_{11} + \frac{1}{\lambda_{SR_n} \xi_{R_n}}} \text{Ei}(-\Delta_{11}) - \Delta_9 e^{\Delta_9 - \frac{\varsigma_{R_n}}{\lambda_{SR_n} \gamma}} \text{Ei}(-\Delta_9), \quad (\text{B.7})$$

$$\begin{aligned}
I_{32} &= \frac{\gamma_{thc}^{R_n} \pi}{N \lambda_{TR_n} \lambda_{ST} \gamma_{thc}^{R_n}} \sum_{k=0}^N K_0 \left(2\sqrt{\Delta_{10}} \right) \sqrt{1 - \vartheta_k^2} \times \\
&\quad \left[e^{-\left(\varsigma_{R_n} B_{R_n} \Delta_{10} + \frac{\varsigma_{R_n}}{\lambda_{SR_n} \gamma} \right)} - e^{-\frac{1}{\lambda_{SR_n} \gamma \xi_{R_n}} - \frac{\vartheta_k + 1}{2\lambda_{SR_n} \gamma \xi_{R_n}}} \right]. \quad (\text{B.8})
\end{aligned}$$

Similarly, substituting (B.7) and (B.8) into (B.6), we can obtain $P_{out}^{T, id}$.

$$\begin{aligned}
P_{out}^{T,id} &= 1 - \int_{\frac{(\psi_{R_n+1/\gamma})\gamma_{thc}^{R_n}}{\Delta_5^{R_n}}}^{\infty} \left(e^{-\frac{\varsigma_{R_n}(B_{R_n}y+\psi_{R_n})}{\lambda_{SR_n}}} - e^{-\frac{\Delta_5^{R_n}y - (\psi_{R_n+1/\gamma})\gamma_{thc}^{R_n}}{\lambda_{SR_n}\xi_{R_n}\gamma_{thc}^{R_n}}} \right) \frac{2}{\lambda_{ST}\lambda_{TR_n}} K_0 \left(2\sqrt{\frac{y}{\lambda_{ST}\lambda_{TR_n}}} \right) dy \\
&= 1 - \underbrace{\int_0^{\infty} \left(e^{-\frac{\varsigma_{R_n}(B_{R_n}y+\psi_{R_n})}{\lambda_{SR_n}}} - e^{-\frac{\Delta_5^{R_n}y - (\psi_{R_n+1/\gamma})\gamma_{thc}^{R_n}}{\lambda_{SR_n}\xi_{R_n}\gamma_{thc}^{R_n}}} \right) \frac{2}{\lambda_{ST}\lambda_{TR_n}} K_0 \left(2\sqrt{\frac{y}{\lambda_{ST}\lambda_{TR_n}}} \right) dy}_{I_{31}} \\
&\quad + \underbrace{\int_0^{\frac{(\psi_{R_n+1/\gamma})\gamma_{thc}^{R_n}}{\Delta_5^{R_n}}} \left(e^{-\frac{\varsigma_{R_n}(B_{R_n}y+\psi_{R_n})}{\lambda_{SR_n}}} - e^{-\frac{\Delta_5^{R_n}y - (\psi_{R_n+1/\gamma})\gamma_{thc}^{R_n}}{\lambda_{SR_n}\xi_{R_n}\gamma_{thc}^{R_n}}} \right) \frac{2}{\lambda_{ST}\lambda_{TR_n}} K_0 \left(2\sqrt{\frac{y}{\lambda_{ST}\lambda_{TR_n}}} \right) dy}_{I_{32}}. \tag{B.6}
\end{aligned}$$

APPENDIX C: PROOF OF THEOREM 4

According to I_1 , we can obtain $P_{int}^{R_f}$ and $P_{int}^{R_n}$. Substituting (5) into (24), the IP of T can be expressed as

- Non-ideal conditions

$$\begin{aligned}
P_{int}^{T,ni} &= \int_{\frac{C_E\gamma_{thc}^E}{\Delta_5^E}}^{\infty} \int_{\frac{M_E\gamma_{thc}^E z + (\psi_{E+1/\gamma})\gamma_{thc}^E}{\Delta_5^E z - C_E\gamma_{thc}^E}}^{\infty} \frac{1}{\lambda_{TE}\lambda_{ST}} e^{-\left(\frac{y}{\lambda_{TE}} + \frac{z}{\lambda_{ST}}\right)} dy dz - \\
&\quad \int_{\frac{C_E\gamma_{thc}^E}{\Delta_5^E}}^{\infty} \int_{\frac{M_E\gamma_{thc}^E z + (\psi_{E+1/\gamma})\gamma_{thc}^E}{\Delta_5^E z - C_E\gamma_{thc}^E}}^{\infty} e^{-\frac{(\Delta_5^E z - C_E\gamma_{thc}^E)y - M_E\gamma_{thc}^E z - (\psi_{E+1/\gamma})\gamma_{thc}^E}{\lambda_{SE}\xi_E\gamma_{thc}^E}} \\
&\quad \times \frac{1}{\lambda_{TE}} e^{-\frac{y}{\lambda_{TE}}} \frac{1}{\lambda_{ST}} e^{-\frac{z}{\lambda_{ST}}} dy dz. \tag{C.1}
\end{aligned}$$

Similar to the derivation process of I_{22} , after some mathematical manipulations, $P_{int}^{T,ni}$ can be obtained.

- Ideal conditions

Substituting $\kappa = 0$ and $\sigma_e^2 = 0$ into (5), $C_E = M_E = 0$. Then, the IP of T at the ideal conditions is given by

$$\begin{aligned}
P_{int}^{T,id} &= \int_0^{\infty} \int_{\frac{\gamma_{thc}^E}{\Delta_5^E}}^{\infty} \left(1 - e^{-\frac{\Delta_5^E\gamma y - \gamma_{thc}^E}{\lambda_{SE}\xi_E\gamma_{thc}^E}} \right) \\
&\quad \frac{2}{\lambda_{TE}\lambda_{ST}} K_0 \left(2\sqrt{\frac{y}{\lambda_{TE}\lambda_{ST}}} \right) dy, \tag{C.2}
\end{aligned}$$

After some mathematical manipulations, we can obtain $P_{int}^{T,id}$.

REFERENCES

- [1] X. Liu, H. Ding, and S. Hu, "Uplink Resource Allocation for NOMA-based Hybrid Spectrum Access in 6G-enabled Cognitive Internet of Things," *IEEE Internet of Things Journal*, pp. 1–1, 2020.
- [2] S. Jacob, V. G. Menon, S. Joseph, P. G. Vinoy, A. Jolfaci, J. Lukose, and G. Raja, "A Novel Spectrum Sharing Scheme using Dynamic Long Short-Term Memory with CP-OFDMA in 5G Networks," *IEEE Transactions on Cognitive Communications and Networking*, pp. 1–1, 2020.
- [3] Y. Liu, Z. Qin, M. Elkashlan, A. Nallanathan, and J. A. McCann, "Non-Orthogonal Multiple Access in Large-Scale Heterogeneous Networks," *IEEE Journal on Selected Areas in Communications*, vol. 35, no. 12, pp. 2667–2680, Dec. 2017.
- [4] M. Zeng, A. Yadav, O. A. Dobre, G. I. Tsiropoulos, and H. V. Poor, "Capacity Comparison Between MIMO-NOMA and MIMO-OMA With Multiple Users in a Cluster," *IEEE Journal on Selected Areas in Communications*, vol. 35, no. 10, pp. 2413–2424, Oct. 2017.
- [5] X. Li, J. Li, Y. Liu, Z. Ding, and A. Nallanathan, "Residual Transceiver Hardware Impairments on Cooperative NOMA Networks," *IEEE Transactions on Wireless Communications*, vol. 19, no. 1, pp. 680–695, Jan. 2020.
- [6] J. Choi, "Power Allocation for Max-Sum Rate and Max-Min Rate Proportional Fairness in NOMA," *IEEE Communications Letters*, vol. 20, no. 10, pp. 2055–2058, Oct. 2016.
- [7] X. Lu, D. Niyato, H. Jiang, D. I. Kim, Y. Xiao, and Z. Han, "Ambient Backscatter Assisted Wireless Powered Communications," *IEEE Wireless Communications*, vol. 25, no. 2, pp. 170–177, Apr. 2018.
- [8] B. Lyu, Z. Yang, H. Guo, F. Tian, and G. Gui, "Relay Cooperation Enhanced Backscatter Communication for Internet-of-Things," *IEEE Internet of Things Journal*, vol. 6, no. 2, pp. 2860–2871, Apr. 2019.
- [9] X. Lu, D. Niyato, H. Jiang, E. Hossain, and P. Wang, "Ambient Backscatter-Assisted Wireless-Powered Relaying," *IEEE Transactions on Green Communications and Networking*, vol. 3, no. 4, pp. 1087–1105, Dec. 2019.
- [10] V. Liu, A. Parks, V. Talla, S. Gollakota, D. Wetherall, and J. R. Smith, "Ambient Backscatter: Wireless Communication out of Thin Air," *ACM SIGCOMM*, vol. 43, no. 4, pp. 39–50, Aug. 2013.
- [11] D. Darsena, G. Gelli, and F. Verde, "Modeling and Performance Analysis of Wireless Networks With Ambient Backscatter Devices," *IEEE Transactions on Communications*, vol. 65, no. 4, pp. 1797–1814, Apr. 2017.
- [12] W. Zhao, G. Wang, S. Atapattu, C. Tellambura, and H. Guan, "Outage Analysis of Ambient Backscatter Communication Systems," *IEEE Communications Letters*, vol. 22, no. 8, pp. 1736–1739, Aug. 2018.
- [13] J. Guo, X. Zhou, S. Durrani, and H. Yanikomeroglu, "Design of Non-Orthogonal Multiple Access Enhanced Backscatter Communication," *IEEE Trans. Wireless Commun.*, vol. 17, no. 10, pp. 6837–6852, Oct. 2018.
- [14] H. Guo, Y. Liang, R. Long, and Q. Zhang, "Cooperative Ambient Backscatter System: A Symbiotic Radio Paradigm for Passive IoT," *IEEE Wireless Communications Letters*, vol. 8, no. 4, pp. 1191–1194, Aug. 2019.
- [15] Y. Ye, L. Shi, X. Chu, and G. Lu, "On the Outage Performance of Ambient Backscatter Communications," *IEEE Internet of Things Journal*, pp. 1–1, 2020.
- [16] X. Li, M. Huang, Y. Liu, V. G. Menon, A. Paul, and Z. Ding, "I/Q Imbalance Aware Nonlinear Wireless-Powered Relaying of B5G Networks: Security and Reliability Analysis," *arXiv preprint arXiv:2006.03902*, 2020. [Online]. Available: <https://arxiv.org/abs/2006.03902>.
- [17] M. Abbasi, A. Shokrollahi, M. R. Khosravi, and V. G. Menon, "High-Performance Flow Classification using Hybrid Clusters in Software Defined Mobile Edge Computing," *Computer Communications*, 2020. doi: 10.1016/j.comcom.2020.07.002.
- [18] A. D. Wyner, "The Wire-tap Channel," *The Bell System Technical Journal*, vol. 54, no. 8, pp. 1355–1387, Oct. 1975.
- [19] N. Nguyen, M. Zeng, O. A. Dobre, and H. V. Poor, "Securing Massive MIMO-NOMA Networks with ZF Beamforming and Artificial Noise," in *2019 IEEE Global Communications Conference (GLOBECOM)*, Feb. 2019, pp. 1–6.
- [20] H. Lei, Z. Yang, K. Park, I. S. Ansari, Y. Guo, G. Pan, and M. Alouini, "Secrecy Outage Analysis for Cooperative NOMA Systems With Relay Selection Schemes," *IEEE Transactions on Communications*, vol. 67, no. 9, pp. 6282–6298, Sept. 2019.

- [21] B. Li, X. Qi, K. Huang, Z. Fei, F. Zhou, and R. Q. Hu, "Security-Reliability Tradeoff Analysis for Cooperative NOMA in Cognitive Radio Networks," *IEEE Transactions on Communications*, vol. 67, no. 1, pp. 83–96, Jan. 2019.
- [22] Q. Yang, H. Wang, Q. Yin, and A. L. Swindlehurst, "Exploiting Randomized Continuous Wave in Secure Backscatter Communications," *IEEE Internet of Things Journal*, vol. 7, no. 4, pp. 3389–3403, Apr. 2020.
- [23] Y. Zhang, F. Gao, L. Fan, X. Lei, and G. K. Karagiannis, "Secure Communications for Multi-Tag Backscatter Systems," *IEEE Wireless Commun. Lett.*, vol. 8, no. 4, pp. 1146–1149, Aug. 2019.
- [24] J. Y. Han, M. J. Kim, J. Kim, and S. M. Kim, "Physical Layer Security in Multi-Tag Ambient Backscatter Communications C Jamming vs. Cooperation," in *2020 IEEE Wireless Communications and Networking Conference (WCNC)*, 2020, pp. 1–6.
- [25] M. Zeng, N. Nguyen, O. A. Dobre, and H. V. Poor, "Securing Downlink Massive MIMO-NOMA Networks With Artificial Noise," *IEEE Journal of Selected Topics in Signal Processing*, vol. 13, no. 3, pp. 685–699, Jun. 2019.
- [26] E. Björnson, J. Hoydis, M. Kountouris, and M. Debbah, "Massive MIMO Systems With Non-Ideal Hardware: Energy Efficiency, Estimation, and Capacity Limits," *IEEE Transactions on Information Theory*, vol. 60, no. 11, pp. 7112–7139, Nov. 2014.
- [27] X. Li, M. Zhao, Y. Liu, L. Li, Z. Ding, and A. Nallanathan, "Secrecy Analysis of Ambient Backscatter NOMA Systems under I/Q Imbalance," *IEEE Transactions on Vehicular Technology*, pp. 1–1, 2020.
- [28] X. Li, Q. Wang, Y. Liu, T. A. Tsiftsis, Z. Ding, and A. Nallanathan, "UAV-Aided Multi-Way NOMA Networks with Residual Hardware Impairments," *IEEE Wireless Communications Letters*, pp. 1–1, 2020.
- [29] P. K. Sharma and P. K. Upadhyay, "Cognitive Relaying With Transceiver Hardware Impairments Under Interference Constraints," *IEEE Communications Letters*, vol. 20, no. 4, pp. 820–823, Apr. 2016.
- [30] J. Cui, Z. Ding, and P. Fan, "Outage Probability Constrained MIMO-NOMA Designs Under Imperfect CSI," *IEEE Transactions on Wireless Communications*, vol. 17, no. 12, pp. 8239–8255, Dec. 2018.
- [31] S. Lee, T. Q. Duong, and R. Woods, "Impact of Wireless Backhaul Unreliability and Imperfect Channel Estimation on Opportunistic NOMA," *IEEE Transactions on Vehicular Technology*, vol. 68, no. 11, pp. 10 822–10 833, Nov. 2019.
- [32] J. He, Z. Tang, Z. Tang, H. Chen, and C. Ling, "Design and Optimization of Scheduling and Non-Orthogonal Multiple Access Algorithms With Imperfect Channel State Information," *IEEE Transactions on Vehicular Technology*, vol. 67, no. 11, pp. 10 800–10 814, Nov. 2018.
- [33] A. K. Mishra, D. Mallick, and P. Singh, "Combined Effect of RF Impairment and CEE on the Performance of Dual-Hop Fixed-Gain AF Relaying," *IEEE Communications Letters*, vol. 20, no. 9, pp. 1725–1728, Sept. 2016.
- [34] X. Li, M. Huang, J. Li, Q. Yu, K. Rabie, and C. C. Cavalcante, "Secure Analysis of Multi-antenna Cooperative Networks with Residual Transceiver HIs and CEEs," *IET Communications*, vol. 13, no. 17, pp. 2649–2659, Oct. 2019.
- [35] X. Ding, T. Song, Y. Zou, X. Chen, and L. Hanzo, "Security-Reliability Tradeoff Analysis of Artificial Noise Aided Two-Way Opportunistic Relay Selection," *IEEE Transactions on Vehicular Technology*, vol. 66, no. 5, pp. 3930–3941, May 2017.
- [36] Taesang Yoo and A. Goldsmith, "Capacity and Power Allocation for Fading MIMO Channels with Channel Estimation Error," *IEEE Transactions on Information Theory*, vol. 52, no. 5, pp. 2203–2214, May 2006.
- [37] S. Stefania, B. Matthew, and T. Issam, *LTE-the UMTS Long Term Evolution: From Theory to Practice*, 2nd ed. New York, NY, USA: Wiley & Sons, 2011.
- [38] M. Abramowitz and I. A. Stegun, *Handbook of Mathematical Functions with Formulas, Graphs, and Mathematical Tables*, 10th ed. New York, NY, USA: Academic, 1972.
- [39] Biglieri, Ezio and Calderbank, Robert and Constantinides, Anthony and Goldsmith, Andrea and Paulraj, Arogyaswami and Poor, H Vincent, *MIMO Wireless Communications*. Cambridge university press, 2007.
- [40] X. Li, M. Zhao, X. Gao, L. Li, D. Do, K. M. Rabie, and R. Kharel, "Physical Layer Security of Cooperative NOMA for IoT Networks Under I/Q Imbalance," *IEEE Access*, vol. 8, pp. 51 189–51 199, Mar. 2020.
- [41] I. S. Gradshteyn and I. M. Ryzhik, *Table of Integrals, Series, and Products*. New York, NY, USA: Academic Press, 2007.
- [42] F. B. Hildebrand, *Introduction to Numerical Analysis*. New York, USA: Dover Publications, 1987.